Direct photon production in $p + p$ collisions at $\sqrt{s} = 200$ GeV at midrapidity

A. Adare,[11] S. Afanasiev,[26] C. Aidala,[36] N. N. Ajitanand,[53] Y. Akiba,[47,48] H. Al-Bataineh,[42] J. Alexander,[53] K. Aoki,[30,47] L. Aphecetche,[55] J. Asai,[47] E. T. Atomssa,[31] R. Averbeck,[54] T. C. Awes,[43] B. Azmoun,[6] V. Babintsev,[21] M. Bai,[5] G. Baksay,[17] L. Baksay,[17] A. Baldisseri,[14] K. N. Barish,[7] P. D. Barnes,[33,*] B. Bassalleck,[41] A. T. Basye,[1] S. Bathe,[7] S. Batsouli,[43] V. Baublis,[46] C. Baumann,[37] A. Bazilevsky,[6] S. Belikov,[6,*] R. Bennett,[54] A. Berdnikov,[50] Y. Berdnikov,[50] A. A. Bickley,[11] J. G. Boissevain,[33] H. Borel,[14] K. Boyle,[54] M. L. Brooks,[33] H. Buesching,[6] V. Bumazhnov,[21] G. Bunce,[6,48] S. Butsyk,[33] C. M. Camacho,[33] S. Campbell,[54] B. S. Chang,[63] W. C. Chang,[2] J.-L. Charvet,[14] S. Chernichenko,[21] C. Y. Chi,[12] M. Chiu,[22] I. J. Choi,[63] R. K. Choudhury,[4] T. Chujo,[58] P. Chung,[53] A. Churyn,[21] V. Cianciolo,[43] Z. Citron,[54] B. A. Cole,[12] P. Constantin,[33] M. Csanád,[16] T. Csörgő,[62] T. Dahms,[54] S. Dairaku,[30,47] K. Das,[18] G. David,[6] A. Denisov,[21] D. d'Enterria,[31] A. Deshpande,[48,54] E. J. Desmond,[6] O. Dietzsch,[51] A. Dion,[54] M. Donadelli,[51] O. Drapier,[31] A. Drees,[54] K. A. Drees,[5] A. K. Dubey,[61] A. Durum,[21] D. Dutta,[4] V. Dzhordzhadze,[7] Y. V. Efremenko,[43] F. Ellinghaus,[11] T. Engelmore,[12] A. Enokizono,[32] H. En'yo,[47,48] S. Esumi,[58] K. O. Eyser,[7] B. Fadem,[38] D. E. Fields,[41,48] M. Finger,[8] M. Finger, Jr.,[8] F. Fleuret,[31] S. L. Fokin,[29] Z. Fraenkel,[61,*] J. E. Frantz,[54] A. Franz,[6] A. D. Frawley,[18] K. Fujiwara,[47] Y. Fukao,[30,47] T. Fusayasu,[40] I. Garishvili,[56] A. Glenn,[11] H. Gong,[54] M. Gonin,[31] J. Gosset,[14] Y. Goto,[47,48] R. Granier de Cassagnac,[31] N. Grau,[12] S. V. Greene,[59] M. Grosse Perdekamp,[22,48] T. Gunji,[10] H.-Å. Gustafsson,[35,*] A. Hadj Henni,[55] J. S. Haggerty,[6] H. Hamagaki,[10] R. Han,[45] E. P. Hartouni,[32] K. Haruna,[20] E. Haslum,[35] R. Hayano,[10] X. He,[19] M. Heffner,[32] T. K. Hemmick,[54] T. Hester,[7] J. C. Hill,[25] M. Hohlmann,[17] W. Holzmann,[53] K. Homma,[20] B. Hong,[28] T. Horaguchi,[10,47,57] D. Hornback,[56] S. Huang,[59] T. Ichihara,[47,48] R. Ichimiya,[47] H. Iinuma,[30,47] Y. Ikeda,[58] K. Imai,[30,47] J. Imrek,[15] M. Inaba,[58] D. Isenhower,[1] M. Ishihara,[47] T. Isobe,[10,47] M. Issah,[53] A. Isupov,[26] D. Ivanischev,[46] B. V. Jacak,[54,†] J. Jia,[12] J. Jin,[12] B. M. Johnson,[6] K. S. Joo,[39] D. Jouan,[44] F. Kajihara,[10] S. Kametani,[47] N. Kamihara,[48] J. Kamin,[54] J. H. Kang,[63] J. Kapustinsky,[33] D. Kawall,[36,48] A. V. Kazantsev,[29] T. Kempel,[25] A. Khanzadeev,[46] K. M. Kijima,[20] J. Kikuchi,[60] B. I. Kim,[28] D. H. Kim,[39] D. J. Kim,[63] E. Kim,[52] S. H. Kim,[63] E. Kinney,[11] K. Kiriluk,[11] Á. Kiss,[16] E. Kistenev,[6] J. Klay,[32] C. Klein-Boesing,[37] L. Kochenda,[46] B. Komkov,[46] M. Konno,[58] J. Koster,[22] A. Kozlov,[61] A. Král,[13] A. Kravitz,[12] G. J. Kunde,[33] K. Kurita,[47,49] M. Kurosawa,[47] M. J. Kweon,[28] Y. Kwon,[56] G. S. Kyle,[42] R. Lacey,[53] Y. S. Lai,[12] J. G. Lajoie,[25] D. Layton,[22] A. Lebedev,[25] D. M. Lee,[33] K. B. Lee,[28] T. Lee,[52] M. J. Leitch,[33] M. A. L. Leite,[51] B. Lenzi,[51] X. Li,[9] P. Liebing,[48] T. Liška,[13] A. Litvinenko,[26] H. Liu,[42] M. X. Liu,[33] B. Love,[59] D. Lynch,[6] C. F. Maguire,[59] Y. I. Makdisi,[5] A. Malakhov,[26] M. D. Malik,[41] V. I. Manko,[29] E. Mannel,[12] Y. Mao,[45,47] L. Mašek,[8,24] H. Masui,[58] F. Matathias,[12] M. McCumber,[54] P. L. McGaughey,[33] N. Means,[54] B. Meredith,[22] Y. Miake,[58] P. Mikeš,[24] K. Miki,[58] A. Milov,[6] M. Mishra,[3] J. T. Mitchell,[6] A. K. Mohanty,[4] Y. Morino,[10] A. Morreale,[7] D. P. Morrison,[6] T. V. Moukhanova,[29] D. Mukhopadhyay,[59] J. Murata,[47,49] S. Nagamiya,[27] J. L. Nagle,[11] M. Naglis,[61] M. I. Nagy,[16] I. Nakagawa,[47,48] Y. Nakamiya,[20] T. Nakamura,[20] K. Nakano,[47,57] J. Newby,[32] M. Nguyen,[54] T. Niita,[58] R. Nouicer,[6] A. S. Nyanin,[29] E. O'Brien,[6] S. X. Oda,[10] C. A. Ogilvie,[25] M. Oka,[58] K. Okada,[48] Y. Onuki,[47] A. Oskarsson,[35] M. Ouchida,[20] K. Ozawa,[10] R. Pak,[6] A. P. T. Palounek,[33] V. Pantuev,[23,54] V. Papavassiliou,[42] J. Park,[52] W. J. Park,[28] S. F. Pate,[42] H. Pei,[25] J.-C. Peng,[22] H. Pereira,[14] V. Peresedov,[26] D. Yu. Peressounko,[29] C. Pinkenburg,[6] M. L. Purschke,[6] A. K. Purwar,[33] H. Qu,[19] J. Rak,[41] A. Rakotozafindrabe,[31] I. Ravinovich,[61] K. F. Read,[43,56] S. Rembeczki,[17] K. Reygers,[37] V. Riabov,[46] Y. Riabov,[46] D. Roach,[59] G. Roche,[34] S. D. Rolnick,[7] M. Rosati,[25] S. S. E. Rosendahl,[35] P. Rosnet,[34] P. Rukoyatkin,[26] P. Ružička,[24] V. L. Rykov,[47] B. Sahlmueller,[37,54] N. Saito,[30,47,48] T. Sakaguchi,[6] S. Sakai,[58] K. Sakashita,[47,57] V. Samsonov,[46] T. Sato,[58] S. Sawada,[27] K. Sedgwick,[7] J. Seele,[11] R. Seidl,[22] A. Yu. Semenov,[25] V. Semenov,[21] R. Seto,[7] D. Sharma,[61] I. Shein,[21] T.-A. Shibata,[47,57] K. Shigaki,[20] M. Shimomura,[58] K. Shoji,[30,47] P. Shukla,[4] A. Sickles,[6] C. L. Silva,[51] D. Silvermyr,[43] C. Silvestre,[14] K. S. Sim,[28] B. K. Singh,[3] C. P. Singh,[3] V. Singh,[3] M. Slunečka,[8] A. Soldatov,[21] R. A. Soltz,[32] W. E. Sondheim,[33] S. P. Sorensen,[56] I. V. Sourikova,[6] F. Staley,[14] P. W. Stankus,[43] E. Stenlund,[35] M. Stepanov,[42] A. Ster,[62] S. P. Stoll,[6] T. Sugitate,[20] C. Suire,[44] A. Sukhanov,[6] J. Sziklai,[62] E. M. Takagui,[51] A. Taketani,[47,48] R. Tanabe,[58] Y. Tanaka,[40] K. Tanida,[47,48,52] M. J. Tannenbaum,[6] A. Taranenko,[53] P. Tarján,[15] H. Themann,[54] T. L. Thomas,[41] M. Togawa,[30,47] A. Toia,[54] L. Tomášek,[24] Y. Tomita,[58] H. Torii,[20,47] R. S. Towell,[1] V-N. Tram,[31] I. Tserruya,[61] Y. Tsuchimoto,[20] C. Vale,[25] H. Valle,[59] H. W. van Hecke,[33] A. Veicht,[22] J. Velkovska,[59] R. Vértesi,[15] A. A. Vinogradov,[29] M. Virius,[13] V. Vrba,[24] E. Vznuzdaev,[46] X. R. Wang,[42] Y. Watanabe,[47,48] F. Wei,[25] J. Wessels,[37] S. N. White,[6] D. Winter,[12] C. L. Woody,[6] M. Wysocki,[11] W. Xie,[48] Y. L. Yamaguchi,[60] K. Yamaura,[20] R. Yang,[22] A. Yanovich,[21] J. Ying,[19] S. Yokkaichi,[47,48] G. R. Young,[43] I. Younus,[41] I. E. Yushmanov,[29] W. A. Zajc,[12] O. Zaudtke,[37] C. Zhang,[43] S. Zhou,[9] and L. Zolin[26]

 © 2012 American Physical Society

(PHENIX Collaboration)

[1]Abilene Christian University, Abilene, Texas 79699, USA
[2]Institute of Physics, Academia Sinica, Taipei 11529, Taiwan
[3]Department of Physics, Banaras Hindu University, Varanasi 221005, India
[4]Bhabha Atomic Research Centre, Bombay 400 085, India
[5]Collider-Accelerator Department, Brookhaven National Laboratory, Upton, New York 11973-5000, USA
[6]Physics Department, Brookhaven National Laboratory, Upton, New York 11973-5000, USA
[7]University of California Riverside, Riverside, California 92521, USA
[8]Charles University, Ovocný trh 5, Praha 1, 116 36, Prague, Czech Republic
[9]Science and Technology on Nuclear Data Laboratory, China Institute of Atomic Energy, Beijing 102413, Peopels Republic of China
[10]Center for Nuclear Study, Graduate School of Science, University of Tokyo, 7-3-1 Hongo, Bunkyo, Tokyo 113-0033, Japan
[11]University of Colorado, Boulder, Colorado 80309, USA
[12]Columbia University, New York, New York 10027 and Nevis Laboratories, Irvington, New York 10533, USA
[13]Czech Technical University, Zikova 4, 166 36 Prague 6, Czech Republic
[14]Dapnia, CEA Saclay, F-91191, Gif-sur-Yvette, France
[15]Debrecen University, H-4010 Debrecen, Egyetem tér 1, Hungary
[16]ELTE, Eötvös Loránd University, H - 1117 Budapest, Pázmány P. s. 1/A, Hungary
[17]Florida Institute of Technology, Melbourne, Florida 32901, USA
[18]Florida State University, Tallahassee, Florida 32306, USA
[19]Georgia State University, Atlanta, Georgia 30303, USA
[20]Hiroshima University, Kagamiyama, Higashi-Hiroshima 739-8526, Japan
[21]IHEP Protvino, State Research Center of Russian Federation, Institute for High Energy Physics, Protvino, 142281, Russia
[22]University of Illinois at Urbana-Champaign, Urbana, Illinois 61801, USA
[23]Institute for Nuclear Research of the Russian Academy of Sciences, prospekt 60-letiya Oktyabrya 7a, Moscow 117312, Russia
[24]Institute of Physics, Academy of Sciences of the Czech Republic, Na Slovance 2, 182 21 Prague 8, Czech Republic
[25]Iowa State University, Ames, Iowa 50011, USA
[26]Joint Institute for Nuclear Research, 141980 Dubna, Moscow Region, Russia
[27]KEK, High Energy Accelerator Research Organization, Tsukuba, Ibaraki 305-0801, Japan
[28]Korea University, Seoul, 136-701, Korea
[29]Russian Research Center "Kurchatov Institute", Moscow, 123098 Russia
[30]Kyoto University, Kyoto 606-8502, Japan
[31]Laboratoire Leprince-Ringuet, Ecole Polytechnique, CNRS-IN2P3, Route de Saclay, F-91128, Palaiseau, France
[32]Lawrence Livermore National Laboratory, Livermore, California 94550, USA
[33]Los Alamos National Laboratory, Los Alamos, New Mexico 87545, USA
[34]LPC, Université Blaise Pascal, CNRS-IN2P3, Clermont-Fd, 63177 Aubiere Cedex, France
[35]Department of Physics, Lund University, Box 118, SE-221 00 Lund, Sweden
[36]Department of Physics, University of Massachusetts, Amherst, Massachusetts 01003-9337, USA
[37]Institut für Kernphysik, University of Muenster, D-48149 Muenster, Germany
[38]Muhlenberg College, Allentown, Pennsylvania 18104-5586, USA
[39]Myongji University, Yongin, Kyonggido 449-728, Korea
[40]Nagasaki Institute of Applied Science, Nagasaki-shi, Nagasaki 851-0193, Japan
[41]University of New Mexico, Albuquerque, New Mexico 87131, USA
[42]New Mexico State University, Las Cruces, New Mexico 88003, USA
[43]Oak Ridge National Laboratory, Oak Ridge, Tennessee 37831, USA
[44]IPN-Orsay, Universite Paris Sud, CNRS-IN2P3, BP1, F-91406, Orsay, France
[45]Peking University, Beijing 100871, People's Republic of China
[46]PNPI, Petersburg Nuclear Physics Institute, Gatchina, Leningrad Region, 188300, Russia
[47]RIKEN Nishina Center for Accelerator-Based Science, Wako, Saitama 351-0198, Japan
[48]RIKEN BNL Research Center, Brookhaven National Laboratory, Upton, New York 11973-5000, USA
[49]Physics Department, Rikkyo University, 3-34-1 Nishi-Ikebukuro, Toshima, Tokyo 171-8501, Japan
[50]Saint Petersburg State Polytechnic University, St. Petersburg, 195251 Russia
[51]Universidade de São Paulo, Instituto de Física, Caixa Postal 66318, São Paulo CEP05315-970, Brazil
[52]Seoul National University, Seoul, Korea
[53]Chemistry Department, Stony Brook University, SUNY, Stony Brook, New York 11794-3400, USA
[54]Department of Physics and Astronomy, Stony Brook University, SUNY, Stony Brook, New York 11794-3400, USA
[55]SUBATECH (Ecole des Mines de Nantes, CNRS-IN2P3, Université de Nantes) BP 20722 - 44307, Nantes, France
[56]University of Tennessee, Knoxville, Tennessee 37996, USA
[57]Department of Physics, Tokyo Institute of Technology, Oh-okayama, Meguro, Tokyo 152-8551, Japan

[58]Institute of Physics, University of Tsukuba, Tsukuba, Ibaraki 305, Japan
[59]Vanderbilt University, Nashville, Tennessee 37235, USA
[60]Waseda University, Advanced Research Institute for Science and Engineering, 17 Kikui-cho, Shinjuku-ku, Tokyo 162-0044, Japan
[61]Weizmann Institute, Rehovot 76100, Israel
[62]Institute for Particle and Nuclear Physics, Wigner Research Centre for Physics, Hungarian Academy of Sciences (Wigner RCP, RMKI) H-1525 Budapest 114, P.O. Box 49, Budapest, Hungary
[63]Yonsei University, IPAP, Seoul 120-749, Korea
(Received 25 May 2012; published 23 October 2012)

The differential cross section for the production of direct photons in $p + p$ collisions at $\sqrt{s} = 200$ GeV at midrapidity was measured in the PHENIX detector at the Relativistic Heavy Ion Collider. Inclusive direct photons were measured in the transverse momentum range from 5.5–25 GeV/c, extending the range beyond previous measurements. Event structure was studied with an isolation criterion. Next-to-leading-order perturbative-quantum-chromodynamics calculations give a good description of the spectrum. When the cross section is expressed versus x_T, the PHENIX data are seen to be in agreement with measurements from other experiments at different center-of-mass energies.

DOI: 10.1103/PhysRevD.86.072008 PACS numbers: 25.75.Dw

I. INTRODUCTION

Direct photons are defined as photons that do not originate from hadronic decays. In hadron-hadron collisions, direct photons at large transverse momentum (p_T) are predominantly produced by the fundamental quantum chromodynamics (QCD) 2-to-2 hard-scattering subprocesses, $g + q \to \gamma + q$ and $\bar{q} + q \to \gamma + g$, where the former subprocess, which dominates in $p + p$ and $A + A$ collisions, is called "the inverse QCD Compton effect" [1]. This subprocess is one of the most important of the QCD 2-to-2 subprocesses for three reasons:

(1) the photon is the only outgoing particle in fundamental QCD 2-to-2 subprocesses that is a single particle, which can be measured to high precision;
(2) the scattered quark has equal and opposite transverse momentum to the direct photon so that the transverse momentum of the jet from the fragmented quark is also precisely known (modulo k_T or multisoft gluon effects [2]); and
(3) it is directly sensitive to the gluon distribution function of the proton times the distribution function of quarks, which is precisely measured in deeply inelastic lepton-proton scattering.

If both the direct photon with p_T and rapidity y_γ and the away side jet at y_J are detected then, to the extent that the $\bar{q} + q \to \gamma + g$ subprocess can be neglected in $p + p$ collisions due to the predominance of gluons over antiquarks, the jet opposite to the direct photon is a quark [2]. Tagging jets with direct photons provides an excellent method of studying any medium effect on the energy or fragmentation of the outgoing quark [3]. Furthermore, the cross section for $g + q \to \gamma + q$ in LO pQCD [1] in scattering of hadron A from hadron B takes on the simple form for the reaction $A + B \to \gamma + q + X$:

$$\frac{d^3\sigma}{dp_T^2 dy_\gamma dy_J} = x_1 g_A(x_1) F_{2B}(x_2) \frac{\pi\alpha\alpha_s(Q^2)}{3\hat{s}^2} \times \left(\frac{1+\cos\theta^*}{2} + \frac{2}{1+\cos\theta^*}\right) + x_2 g_B(x_2) F_{2A}(x_1) \frac{\pi\alpha\alpha_s(Q^2)}{3\hat{s}^2} \times \left(\frac{1-\cos\theta^*}{2} + \frac{2}{1-\cos\theta^*}\right), \quad (1)$$

where the parton kinematics are fully determined by

$$x_1 = x_T \frac{e^{y_\gamma} + e^{y_J}}{2}, \qquad x_2 = x_T \frac{e^{-y_\gamma} + e^{-y_J}}{2}, \quad (2)$$

and $x_T = 2p_T/\sqrt{s}$. The parton-parton c.m. energy $\sqrt{\hat{s}} = \sqrt{x_1 x_2 s}$, where $\sqrt{s}$ is the $A + B$ c.m. energy; the energy of the direct photon in the parton-parton c.m. system is $P_\gamma^* = E_\gamma^* = \sqrt{\hat{s}}/2$, where

$$p_T = p_T^* = \frac{\sqrt{\hat{s}}}{2} \sin\theta^* \quad (3)$$

and $\cos\theta^* = \tanh(y_\gamma - y_J)/2$ is the c.m. angle of the outgoing γ with respect to hadron A. In Eq. (1), $g_A(x_1, Q^2)$ and $g_B(x_2, Q^2)$ are the gluon structure functions of hadron A and hadron B. At leading order $F_{2A}(x_1, Q^2)$ and $F_{2B}(x_2, Q^2)$ are structure functions measured in deep inelastic scattering (DIS) of $e + A$, given by $F_{2A}(x, Q^2) = x\sum_a e_a^2 f_a^A(x, Q^2)$, where $f_a^A(x, Q^2)$ are the distributions in the number of quarks of type a, with electric charge e_a (in units of the proton charge) in hadron A.[1] In hard $g + q \to \gamma + q$ scattering in $p + p$ collisions, the struck quark is 8 times more likely to be a u quark relative to a d quark.

*Deceased.
†PHENIX spokesperson: jacak@skipper.physics.sunysb.edu

[1]The relation $F_2 = F_2(\mathrm{DIS})$ is true only in leading order pQCD. They can be different in higher order pQCD. But the difference is accounted in the theory.

For production in nuclei, the ratio is somewhat less according to the ratio of the atomic number to the atomic mass.

Beyond leading order, direct photons can be produced either by bremsstrahlung from any quark line in a 2-to-2 subprocess, e.g. $g + q \rightarrow g + q + \gamma$, or in a parton shower from fragmentation that forms a jet. In both these cases the photon is accompanied by jet fragments so that observing photons isolated from jets enhances the contribution from the fundamental 2-to-2 subprocesses. Naturally, all these effects must be taken into account in theoretical calculations of direct photon production in pQCD, and such calculations [4] are generally in excellent agreement with all previous measurements, including those from PHENIX [5]. However, decreasing the uncertainties of both measurement and theory and extending the range to larger p_T is desirable. Measurements with and without an isolation criterion allow more specific comparisons of theoretical models and a better understanding of photons coming from bremsstrahlung and parton fragmentation.

Measurement of direct photons in $p + p$ collisions provides an important baseline for measurements in heavy-ion collisions. Once produced, a photon emerges from the reaction almost unaffected since it only interacts electromagnetically. Initial state modifications of the distribution functions in nuclei can be accessed by measurements in $p + A$ or $d + A$ collisions. Similarly, direct photons provide a reference free from final state effects on the outgoing quark, which at LO initially balances the p_T of the direct photon.

In this paper, we report a major update of the direct photon cross section measurement in $p + p$ collisions at $\sqrt{s} = 200$ GeV. The present data has more than an order of magnitude improved statistics than that reported in [5]. It has extended the highest p_T reach of the measurement from 15 GeV/c to 25 GeV/c. We compare the data to pQCD calculations and other direct photon data in hadronic collisions.

The paper is organized as follows: Section II describes the experimental setup. Section III describes the analysis method. Results are in Sec. IV followed by a discussion (Sec. V) and summary (Sec. VI). The measured invariant cross sections are tabulated in the Appendix.

II. EXPERIMENTAL SETUP

Photons were detected in the PHENIX central arm detectors by two electromagnetic calorimeter (EMCal) arms (west, east) each covering $\pi/2$ rad in azimuthal angle (ϕ) and $|\eta| < 0.35$ in pseudorapidity. Each arm is divided into 4 sectors in azimuth. All 4 sectors in the west arm are lead scintillator sampling detectors (PbSc). In the east arm, 2 sectors are PbSc and 2 sectors are lead glass Čerenkov detectors (PbGl). The sectors are composed of independent towers with granularities of $\Delta\eta \times \Delta\phi = 0.011 \times 0.011$ and 0.008×0.008 for the PbSc and the PbGl, respectively. Photon clusters are composed from the sum of energy deposits in a center tower and adjacent towers. The transverse containment in a single tower hit near the center is $\sim$80%. During data taking, the relative gain of the detectors was monitored using a light pulser calibration system. The absolute energy calibration was based on the known minimum-ionizing energy peak of charged tracks, energy-momentum matching of identified electron tracks, and the measured value of the $\pi^0 \rightarrow \gamma\gamma$ invariant mass. The linearity of the energy response was obtained from beam tests and the dependence of the measured π^0 mass on its momentum. The energy resolution was determined using the width of the π^0 peak, and was $\sigma_E/E = 8.1\%/\sqrt{E}(\mathrm{GeV}) \oplus 5.7\%$. The systematic error on the absolute energy scale is less than 1.5%. The time of flight (ToF) as measured by the EMCal with a resolution of better than 1 ns was used to reduce the cosmic ray background.

The dynamic range of the electronics is saturated for the highest energy clusters ($\sim$ 25 GeV) measured in this analysis. The size of this effect is estimated using a convolution of the maximum energy limit of each tower (26 GeV typical) and the fraction of energy deposited in the central tower of a electromagnetic shower cluster. This effect was found negligible compared to the statistical uncertainty for the very high energy photons that are affected.

The drift chambers (DC) and the innermost layer of the pad chambers provide charged track information and were used to veto charged hadron clusters in the EMCal. Hits in the beam-beam counters (BBCs) positioned at pseudorapidities $3.1 < |\eta| < 3.9$ were used to measure a collision vertex from the time difference between hits in both BBCs, and to monitor the luminosity. The PHENIX detector is described in detail elsewhere [6].

III. ANALYSIS

A. Event selection

The results in this paper are based on the data sample taken during the 2006 RHIC run. A high p_T photon sample was collected with an EMCal trigger in which the analog sum of signals from a 4×4 adjacent set of EMCal towers was greater than a nominal energy threshold of 2 GeV, which was in coincidence with the minimum-bias trigger, corresponding to $\sim$8.0 pb^{-1} integrated luminosity. The integrated luminosity was determined from the rate of a minimum-bias trigger that required hits in the BBCs and a collision vertex within 30 cm of the nominal center of the interaction region. At $\sqrt{s} = 200$ GeV this trigger selects 23.0 mb of the inelastic $p + p$ cross section. This was measured with 9.7% uncertainty using a Vernier-scan technique [7,8]. This corresponds to about 55% of the inelastic $p + p$ cross section. For the BBC trigger rate of 250 kHz typical of the sample used in this analysis in the crossing rate of 9.4 MHz, the effect of multiple collisions per bunch crossing was <2% and is neglected.

B. Photon selection

Photon candidates were reconstructed from EMCal clusters within an EMCal fiducial volume defined to exclude the edge areas $\Delta\eta = 0.10$ and $\Delta\phi = 0.10$ wide, resulting in a fiducial area of $|\eta_f| < 0.25$ in pseudorapidity and $\Delta\phi_f = \pi/2 - 0.2$ in azimuth for each of the two arms. Areas outside the fiducial volume were included when searching for a partner candidate for $\pi^0 \to \gamma\gamma$ decays to suppress π^0 background, and to measure activity around direct photon candidates (an isolation cut, Sec. III E) to suppress bremsstrahlung and fragmentation photons in the reconstructed photon sample.

Photon candidates were required to have $p_T > 5$ GeV/c and a ToF measured by the EMCal to be within ± 5 ns from the expected arrival time for the photons originating at the vertex. This requirement reduced the background from cosmic rays by an order of magnitude. The remaining contributions are estimated from the ToF distribution and corrected. The magnitude of this correction was negligible in the region of $p_T < \sim 15$ GeV/c and larger for higher p_T photons as the rate goes down ($\sim 8\%$ contamination at $p_T = 25$ GeV/c). The background from charged tracks was suppressed by requiring that the EMCal cluster shape be consistent with a single electromagnetic shower and that no charged track points to the cluster. The shower shape cut efficiency for photons, evaluated using reconstructed π^0 decay photons, was 0.98 over the relevant p_T range. Most of the conversion e^+e^- pairs in the $\sim 10\%$ of radiation length of material between the DC and the EMCal are reconstructed as single photons because of the minimal magnetic field in this region. Of course, no charged track would point to the cluster since the conversion would have happened after the DC. An additional 1% loss was attributed to these photon conversions from a GEANT [9] simulation with a reasonable input p_T distribution. The contribution of the other hadronic background (neutrons, K_L, albedo from magnet poles and other material) was studied with a detailed GEANT Monte Carlo simulation and found to be less than 1% of the photon sample.

The fine granularity of the PHENIX EMCal resolves the two photons from $\pi^0 \to \gamma\gamma$ decays up to $\pi^0 p_T$ of 12 GeV/c (17 GeV/c) in the PbSc (PbGl). A 50% merging probability corresponds to $\pi^0 p_T$ of 17 GeV/c (25 GeV/c). In the p_T range presented in this paper (up to 25 GeV/c), merged photons can be separated from single photon showers in the EMCal and rejected using shower shape measurements with an efficiency $>90\%$.

C. Direct photon signal extraction

In the obtained photon sample the majority of the background for direct photon measurements comes from decays of hadrons, primarily $\pi^0 \to \gamma\gamma$ ($\sim 80\%$) and $\eta \to \gamma\gamma$ ($\sim 15\%$). The contribution from π^0 decays was evaluated by a π^0-tagging method.[2] In this approach the direct photon candidate was paired with each of the other photons in an event (a partner photon) to calculate the two-photon invariant mass $M_{\gamma\gamma}$, which was required to be in the range from 105 to 165 MeV corresponding to $\pm 3\sigma$ around the π^0 peak (see Fig. 1). Both photons were required to have a minimum energy $E_{\min} = 0.5$ GeV.

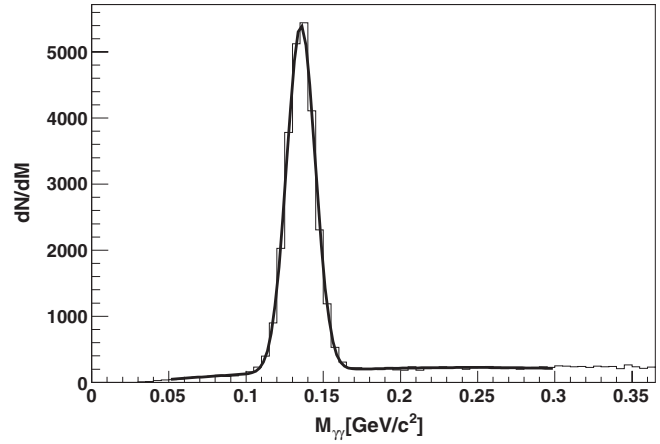

FIG. 1. Two-photon invariant mass distribution in the west arm where one of the photons has $5 < p_T < 5.5$ GeV/c.

The combinatorial background under the π^0 peak was evaluated and then subtracted by fitting the two-photon invariant mass distribution outside the peak region. The corrections for the underestimation due to photon conversions and π^0 Dalitz decays were applied as a part of the partner photon efficiency. To avoid acceptance losses for π^0 reconstruction, the edge areas of the EMCal outside the fiducial region were included for partner photon selection as long as the primary photon was in the fiducial region. The minimum photon energy cut, the EMCal geometry, and inactive areas led to an underestimate of the π^0 decay photon yields. A correction for this was calculated using a single particle Monte Carlo simulation, which included the EMCal geometry, the configuration of dead areas, resolution, and the π^0 spectrum shape from earlier measurements [8]. Figure 2 shows a p_T dependent multiplicative correction, denoted as $1 + R$, to the tagged π^0 photon sample. $1 + R$ drops with increasing p_T when going from 5 GeV/c to 15 GeV/c due to the decreasing influence of the $E_{\min}$ cut. As the p_T increases further the correction stops decreasing due to an increasing merging probability. The correction for asymmetric decays is more affected by the $E_{\min}$ cut, since symmetric decays start merging and are rejected from the photon sample by the shower shape cut. Completely merged photons from high p_T π^0 decays may

[2] In the previous measurement [5], we introduced a π^0-tagging method and a cocktail subtraction method. Both use statistical subtraction, but the π^0-tagging method uses the photon p_T on which it is easier to apply an isolation cut.

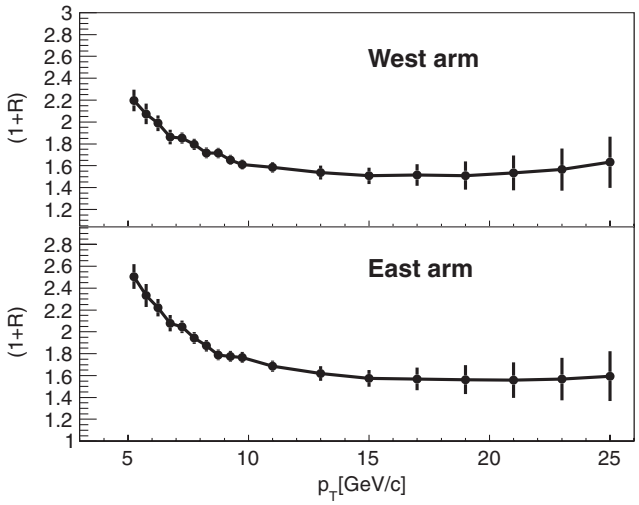

FIG. 2. The correction factor to be applied to the number of tagged photons for the total contribution from π^0 $[(1+R)]$ in Eq. (4)) from a single particle Monte Carlo simulation. The error bar shows the systematic uncertainty.

resemble single photons in the EMCal; this residual contribution is corrected later.

The contribution to the photon sample from hadronic decays other than from π^0s was estimated relative to the π^0 decay contribution based on the η/π^0 [10], and ω/π^0 and η'/π^0 [11] ratios from our measurements assuming m_T scaling (tested in [11]). We denote the ratio of photons from these decays to the photons from π^0 decays as A. At lower p_T ($p_T \sim 5$ GeV/c) this ratio, A, has a weak p_T dependence and approaches 0.235 as p_T increases. Since the contribution of photons from π^0 to the background decreases for $p_T > 10$ GeV/c due to π^0 photons merging, the value, A, starts to rise linearly at around $p_T = 12$ GeV/c, and at the highest p_T point at 25 GeV/c it is 1.4 (0.94) for west (east) arm.

The yield of direct photons $N_{\rm dir}$ was obtained from the inclusive photon yield $N_{\rm incl}$ as follows:

$$N_{\rm dir} = N_{\rm incl} - (1+A)(1+R)N_{\pi^0}, \tag{4}$$

where N_{π^0} is the contribution from π^0s evaluated with a tagging process. In this notation, $(1+R)\cdot N_{\pi^0}$ represents the total contribution from unmerged $\pi^0 \to \gamma\gamma$ decays, and $A\cdot(1+R)\cdot N_{\pi^0}$ is the contribution from other hadronic decays.

Figures 3 and 4 show different contributions to the inclusive photon spectrum separately for west and east spectrometers. In the highest p_T bins, where no π^0-tagged photons were found (due to low statistics and high merging probability), N_{π^0} was set to 0^{+1}_{-0} to safely cover the other hadronic decay channels.

D. Direct photon cross section

Based on the extracted direct photon yields $N_{\rm dir}$ in each Δp_T wide bin in transverse momentum, the invariant cross section of direct photon production was calculated as follows:

$$E\frac{d^3\sigma}{dp^3} = \frac{1}{\mathcal{L}}\frac{1}{2\pi p_T}\frac{N_{\rm dir}}{\Delta p_T \Delta y}\frac{1}{\epsilon}\frac{1}{\epsilon_{\rm bias}}, \tag{5}$$

where $\mathcal{L}$ is the integrated luminosity for the analyzed data sample, Δy is the rapidity range, ϵ corrects for the acceptance including the trigger live area, photon reconstruction efficiency, trigger efficiency, and p_T smearing due to EMCal energy resolution. $\epsilon_{\rm bias}$ corrects for the finite efficiency of BBCs to trigger on high p_T events. The latter was measured from the ratio of π^0 yields obtained using the EMCal based high p_T photon trigger with and without

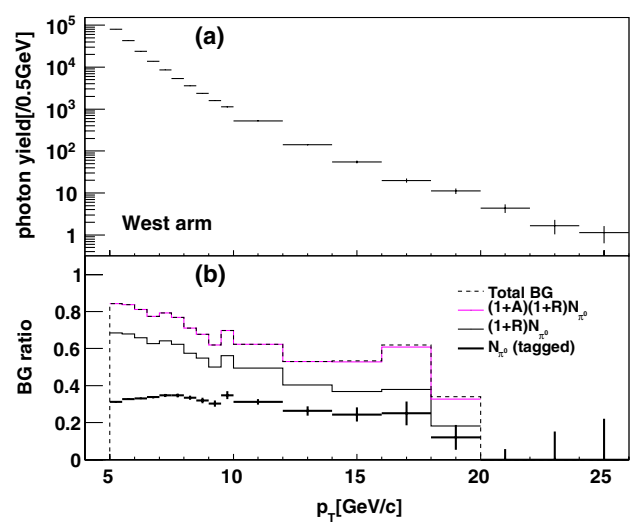

FIG. 3 (color online). In the west arm, (a) number of photon clusters and (b) background-photon fraction. From bottom to top, tagged π^0 (N_{π^0}), total photons from unmerged π^0 ($(1+R)N_{\pi^0}$), all hadronic decay $[(1+A)(1+R)N_{\pi^0}]$, and the total background including an estimate of completely merged clusters. In the highest 3 bins where no π^0-tagged photons were found, only the uncertainties of N_{π^0} are shown.

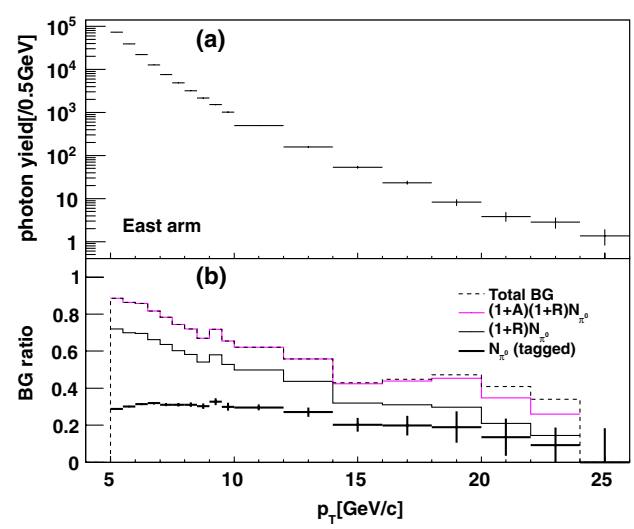

FIG. 4 (color online). The same as Fig. 3 but for the east arm.

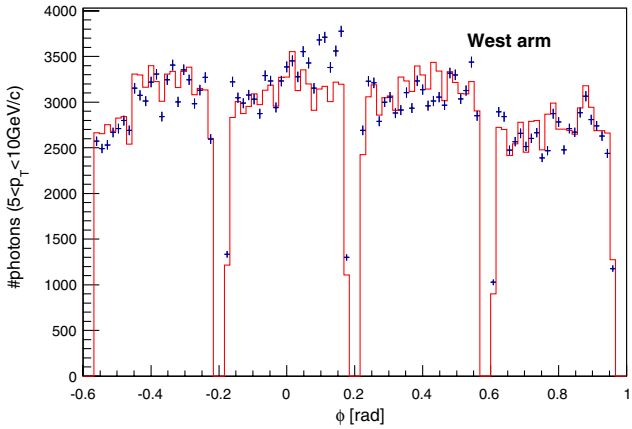

FIG. 5 (color online). Number of photons ($5 < p_T < 10\,\mathrm{GeV}/c$) as a function of the azimuthal angle (west arm). The histogram shows the MC result normalized by the total count.

BBC trigger requirements, and was found to be 0.78 ± 0.02, independent of p_T.

A single particle Monte Carlo simulation, which included the configuration of detector active areas and resolutions, was used to evaluate the corrections for the acceptance and p_T smearing. The small differences between the distribution of azimuthal position of reconstructed photons between data and simulation (Figs. 5 and 6) served to estimate the systematic uncertainty. The effects of p_T smearing were determined by varying the input p_T spectrum of the simulation to cover the uncertainty of the measured spectrum. The same simulation framework was used to evaluate the propagation of the 1.5% scale uncertainty in the EMCal energy measurements to the final direct photon spectrum.

The terms from Eq. (4) used to calculate N_{dir} contribute to its uncertainty as follows (as tabulated in Appendix Table VI):

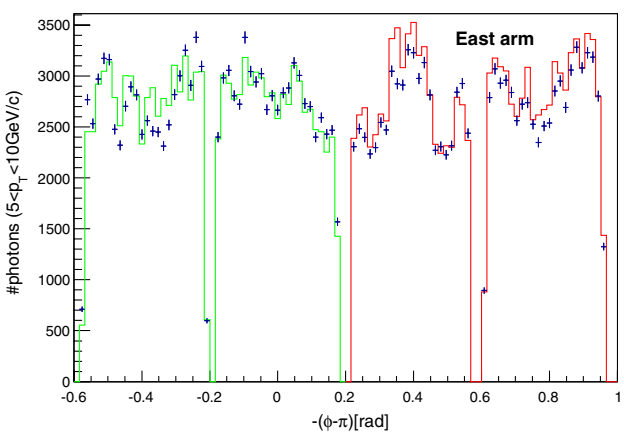

FIG. 6 (color online). Number of photons ($5 < p_T < 10\,\mathrm{GeV}/c$) as a function of the azimuthal angle (east arm). The lower (upper) half corresponds to PbGl (PbSc) sectors. The histogram shows the MC result normalized by the total count (PbSc and PbGl sectors are done separately.)

$$\frac{\delta N_{\mathrm{dir}}}{N_{\mathrm{dir}}} = W \cdot \left(\frac{\delta N_{\mathrm{incl}}}{N_{\mathrm{incl}}}\right) \oplus (W-1) \cdot \left(\frac{\delta(1+A)}{(1+A)}\right) \oplus (W-1) \cdot \left(\frac{\delta(1+R)}{(1+R)}\right) \oplus (W-1) \cdot \left(\frac{\delta N_{\pi^0}}{N_{\pi^0}}\right), \tag{6}$$

where W is defined as $N_{\mathrm{incl}}/N_{\mathrm{dir}}$. At low p_T with high backgrounds ($W \gg 1$), the contributing uncertainties on N_{dir} are amplified by a factor W or $W - 1$. In this p_T range the dominant uncertainty comes from the correction for untagged photons $[(1 + R)]$ from π^0 decay due to its sensitivity to the minimal energy cut, E_{min}. In the higher p_T bins the biggest systematic uncertainty of the component is in the merging effect [which is included in the $(1 + R)$ term], since most of π^0s are merged in the EMCal in this p_T region. However, this effect on the direct photon is small, suppressed by a factor $(W - 1) \ll 1$, because of the small background fraction and approaches zero at highest p_T.

E. Study of the effect of isolation cut

In this section we investigate the effect of an isolation cut on direct photons to determine the fraction coming from Compton and annihilation processes, which are expected to be isolated from jet activity. The energy around the photon candidate in a cone of radius $r = \sqrt{(\delta\eta)^2 + (\delta\phi)^2} = 0.5$ was required to be less than 10% of the photon energy, in order to pass the isolation cut. The cone size is determined by the hadron correlation in a jet measurement (e.g. Fig. 6 in [2]). The total energy in the cone was constructed by summing the energy of electromagnetic clusters in the EMCal and the momentum of charged tracks in the tracking system. To be counted as part of the cone energy, the minimum EMCal cluster energy was set at 0.15 GeV and the minimum track momentum at $0.2\ \mathrm{GeV}/c$, close to the lower limit for charged particle reconstruction in PHENIX. To avoid inclusion of misidentified tracks, which, due to decays or photon conversions may mimic high p_T tracks, the maximum momentum for the tracks to participate in the cone energy calculation was set to $15\ \mathrm{GeV}/c$.

Aside from direct photons, the isolated photon sample ($N_{\mathrm{incl}}^{\mathrm{iso}}$) includes background photons from π^0 and other hadron decays. For π^0 decays we consider photons that have a partner photon reconstructed in the EMCal acceptance ($n_{\pi^0}^{\mathrm{iso}}$), and those which satisfy the isolation criteria if the partner photon is masked out ($N_{\pi^0}^{\mathrm{iso}}$). More π^0 photons pass the isolation cut without the partner photon energy, so $n_{\pi^0}^{\mathrm{iso}}$ is a subgroup of $N_{\pi^0}^{\mathrm{iso}}$. The latter was used to estimate the isolated photons from π^0 with missing partner due to the energy threshold E_{min} or EMCal masked areas, by multiplying by the same missing photon fraction R introduced in Eq. (4).

To estimate the contribution of other hadron decays, the isolated photon candidate from π^0 ($N_{\pi^0}^{\mathrm{iso}}$) is scaled. With

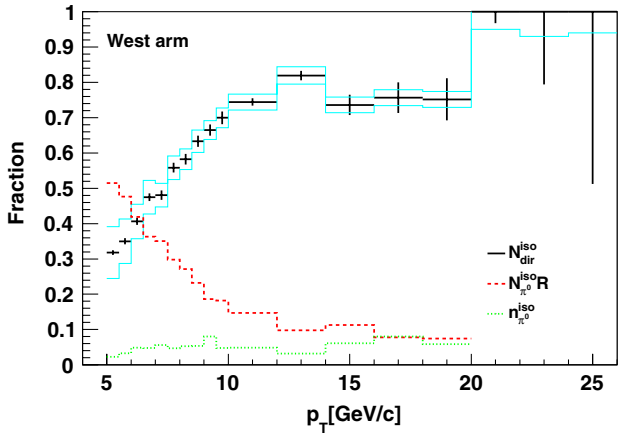

FIG. 7 (color online). Components of isolated photon clusters (west arm). Solid line (with error): isolated direct photon signal ($N^{\rm iso}_{\rm dir}$), Dashed line: photons from π^0 with missing partner ($N^{\rm iso}_{\pi^0}R$), Dotted line: Photons tagged as π^0 ($n^{\rm iso}_{\pi^0}$).

this procedure, the isolation cut efficiency from jet fragments is taken into account; however, there is an additional rejection due to its own partner photon. A single particle MC for ηs was used to include this effect. In the case of ηs, for the lowest p_T sample, the partner photon can be out of the EMCal acceptance because of a large opening angle, thereby reducing the rejection power. As it goes to high p_T, the rejection power due to the partner energy becomes constant.

Similar to Eq. (4), the isolated direct photon yield ($N^{\rm iso}_{\rm dir}$) was calculated using

$$N^{\rm iso}_{\rm dir} = N^{\rm iso}_{\rm incl} - (n^{\rm iso}_{\pi^0} + N^{\rm iso}_{\pi^0}R) - A^{\rm iso}(1+R)N^{\rm iso}_{\pi^0}. \quad (7)$$

In addition to A in Eq. (4), $A^{\rm iso}$ includes the isolation cut effect of the hadron's own partner photon as described above. Different contributors to the isolated photon sample $N^{\rm iso}_{\rm incl}$ are shown in Figs. 7 and 8.

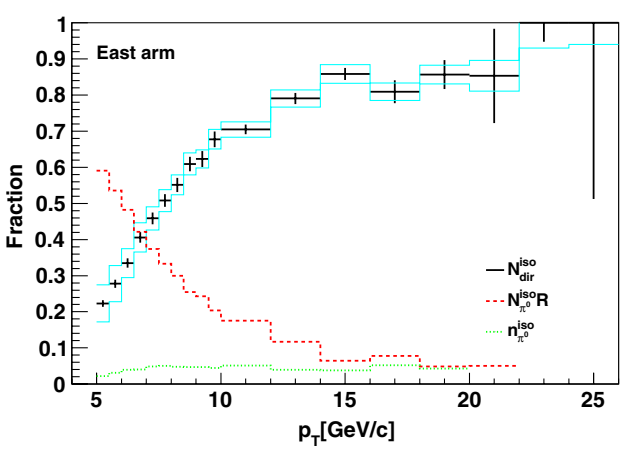

FIG. 8 (color online). Components of isolated photon clusters (east arm).

Uncertainties are propagated according to

$$\frac{\delta N^{\rm iso}_{\rm dir}}{N^{\rm iso}_{\rm dir}} = W_0 \frac{\delta N^{\rm iso}}{N^{\rm iso}_{\rm incl}} \oplus W_1 \frac{\delta(1+A^{\rm iso})}{(1+A^{\rm iso})} \oplus W_1 \frac{\delta(1+R)}{(1+R)} \oplus W_2 \frac{\delta n^{\rm iso}_{\pi^0}}{n^{\rm iso}_{\pi^0}} \oplus W_3 \frac{\delta N^{\rm iso}_{\pi^0}}{N^{\rm iso}_{\pi^0}},$$

$$W_0 = \frac{N^{\rm iso}_{\rm incl}}{N^{\rm iso}_{\rm dir}}, \qquad W_1 = \frac{(1+A^{\rm iso})(1+R)N^{\rm iso}_{\pi^0}}{N^{\rm iso}_{\rm dir}},$$

$$W_2 = \frac{n^{\rm iso}_{\pi^0}}{N^{\rm iso}_{\rm dir}}, \quad \text{and} \quad W_3 = \frac{((1+A^{\rm iso})(1+R)-1)N^{\rm iso}_{\pi^0}}{N^{\rm iso}_{\rm dir}}. \quad (8)$$

Smoothed functions from fits to the data of the W_0, W_1, W_2, and W_3 parameters were used. The overall trend is the same as in the case of inclusive photon measurement. However at low p_T the systematic uncertainties are smaller due to smaller contribution from hadronic decay photons in the isolated photon sample. Appendix Table VII summarizes the systematic uncertainties for isolated direct photon measurements.

F. Isolation over inclusive direct photon ratio

By taking the ratio of isolated direct photons to the inclusive direct photons, some uncertainties such as photon efficiency and the luminosity measurement cancel. To estimate the remaining systematic uncertainty, each component contributing to the yield measurements was moved up and down by $\pm 1\sigma$ of its systematic uncertainty. Figure 9 shows the variation due to this change. The values are tabulated in the Appendix, Table V. The total systematic uncertainty was taken as the quadratic sum of these variations.

To evaluate the rejection power of the isolation cut on jet fragmentation, the same ratio was calculated for photons

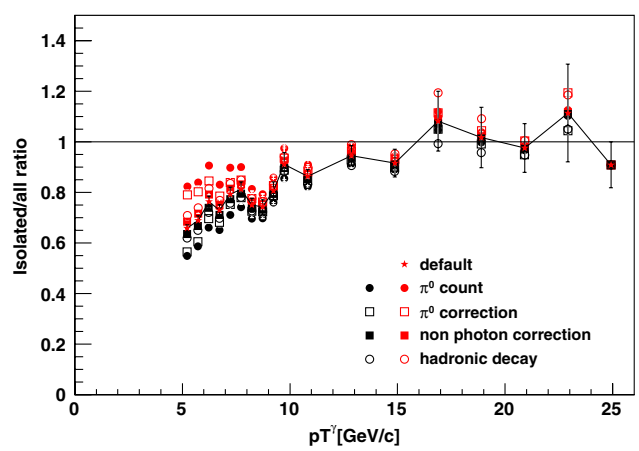

FIG. 9 (color online). Effects in the ratio of isolated direct photons for (black points) -1σ and (red points) $+1\sigma$ of systematic uncertainty change: (closed circles) π^0 counts, (open squares) untagged π^0 corrections, (closed squares) nonphoton contributions, (open circles) hadronic components other than π^0.

from π^0 ($= N^{\rm iso}_{\pi^0}/N_{\pi^0}$). Here the systematic uncertainty is from the correction of combinatorial background.

IV. RESULTS

Figure 10 shows the inclusive direct photon cross section where the bin width correction in the data are applied to the vertical direction. The data are compared to a NLO pQCD calculation [12–17] using the coordinated-theoretical-experimental-project-on-QCD-6 (CTEQ6M) parton distribution functions [18] and the Bourhis-Fontannaz-Guillet (BFGII) [19] parton-to-photon fragmentation function for three different renormalization and factorization scales, from bottom to top, $\mu = 2p_T$, p_T, and $p_T/2$. The deviation of the data from the calculation is shown in the bottom panel. The present data are consistent with that which we previously published in [5]. The highest p_T reach of the data is expanded from 15 GeV/c to 25 GeV/c. For the p_T range ($8 < p_T < 25$ GeV/c) a power law fit to the data gives the power $n = 7.08 \pm 0.09(\text{stat}) \pm 0.1(\text{syst})$ with $\chi^2/\text{NDF} = 8.3/10$. In the fit, all systematic uncertainties are treated as correlated.

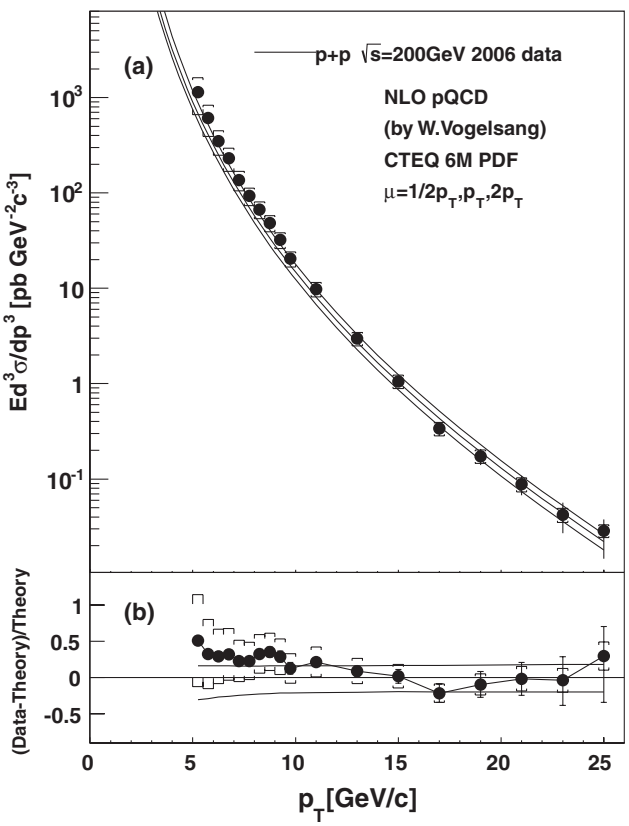

FIG. 10. (a) Inclusive direct photon spectra compared with an NLO pQCD calculation for three different renormalization and factorization scales as mentioned in the text (the same CTEQ6M PDF calculation [18] was used in [5]). The error bars denote point-by-point uncertainties, the error brackets show p_T correlated uncertainties. (b) Comparison of the data and the pQCD calculation.

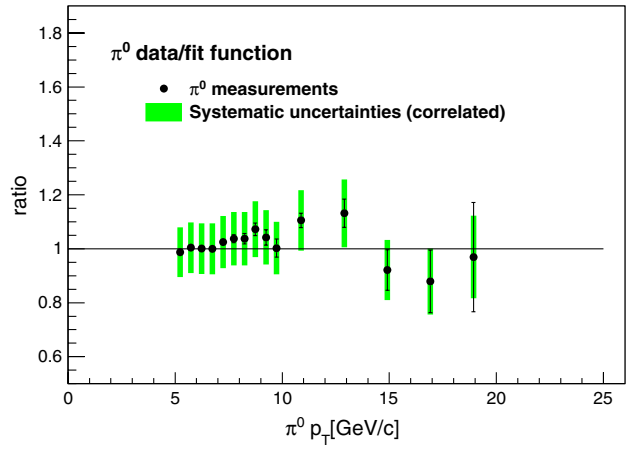

FIG. 11 (color online). The ratio of π^0 spectrum [20] to the power law fit for the range $5 < p_T < 20$ GeV/c. The systematic uncertainty shown by the box does not include the overall normalization uncertainty.

To demonstrate the purity of the signal as a function of photon p_T, ratios to π^0 spectrum are taken. The measured π^0 cross section [20] is parametrized by the form $E\frac{d^3\sigma}{dp^3}\,[\text{pb}] = 1.777 \times 10^{10} p_T^{-8.22}$ as show in Fig. 11. The systematic uncertainty shown with a band does not include the overall normalization uncertainty. Figure 12 shows the ratio of both the direct photon signal and photons from π^0 to the fit. The dotted line in the figure is at $2/(8.22 - 1) = 0.277$, which is the analytic expectation for the ratio of π^0 decay photons to π^0 in case of a pure power law behavior of the π^0. The fraction of the direct photon contribution gets higher as the transverse momentum increases. The

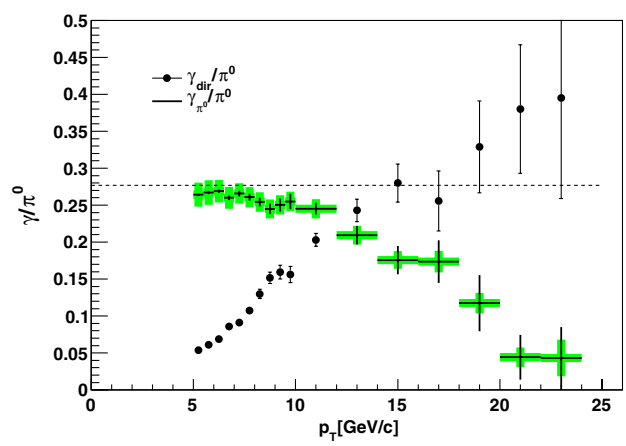

FIG. 12 (color online). The filled circles ($\gamma_{\rm dir}/\pi^0$): the ratio of the direct photon cross section to the π^0 cross section fit. The crosses (γ_{π^0}/π^0): the ratio of the background photon from π^0 decay to the π^0 cross section fit. The π^0 cross section used for the denominator is the fit curve explained in the text and shown in Fig. 11. The dotted line shows the analytical expectation of γ_{π^0}/π^0. See the text for details. The systematic uncertainty on the π^0 photon contribution includes acceptance, smearing, π^0 photon counting, and untagged π^0 photon probability. (These uncertainties enter as A2, C, and D in Appendix Table VI).

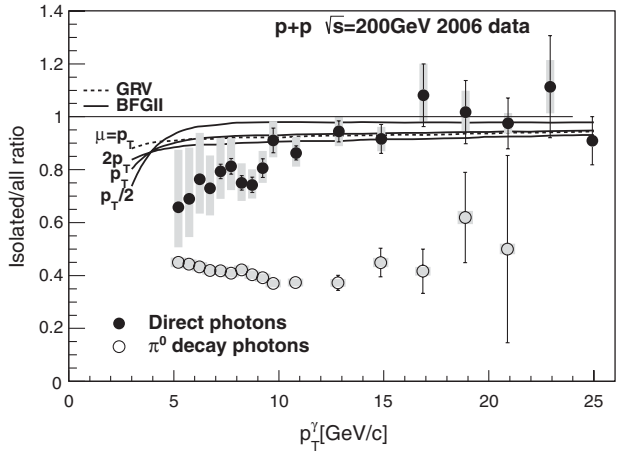

FIG. 13. The effect of isolation cut on direct photons and decay photons. Solid circles: Ratio of isolated direct photons to inclusive direct photons. The statistical uncertainties are shown as black error bars and the systematic uncertainties are plotted as shaded bars. The solid and dashed curves are NLO pQCD calculations with three theory scales for BFGII [19] and one scale for the GRV [21] parton-to-photon fragmentation functions. Open circles: Ratio of isolated photons from π^0 decays to all photons from π^0 decays.

contribution of photons from π^0s deviates from the analytic expectation at higher p_T because most of the merged clusters are rejected from the photon sample. The data are systematically lower than the analytical line even at the lowest p_T. But as shown in Fig. 11, the systematic uncertainty of the fit constant is on the order of 10%. If this uncertainty is taken into account, the agreement is reasonable.

Figure 13 shows the ratio of isolated direct photons to inclusive direct photons, and isolated over inclusive photons from π^0s. Since the background subtractions are done independently, this ratio can exceed unity due to the uncertainty. The data are compared to two theoretical calculations, which include the same isolation criteria. The solid and dashed curves are NLO pQCD calculations with three theory scales for BFGII [19] and one scale for the Gluck-Reya-Vogt (GRV) [21] parton-to-photon fragmentation functions. The cone size of the isolation cut is larger than the area within the PHENIX central arm acceptance around the isolated photon candidate and leads to an underestimate of the energy in the cone. This effect was not corrected for; instead the same acceptance was included in the theory calculation. However the theory calculation assumes no dead areas in the acceptance. The theory calculation varies at most by 2% (90% → 92%), when the effect of the dead area is included.

The isolation cut causes a large suppression of photons from π^0. This is expected as the π^0 is accompanied with other fragmentation products. At high p_T ($p_T > \sim 10\,\mathrm{GeV}/c$), the ratio of isolated direct photon to inclusive direct photons is typically more than 90% and matches the expectation from NLO pQCD calculations. At low p_T, the data are below the theory calculation, although generally they agree within

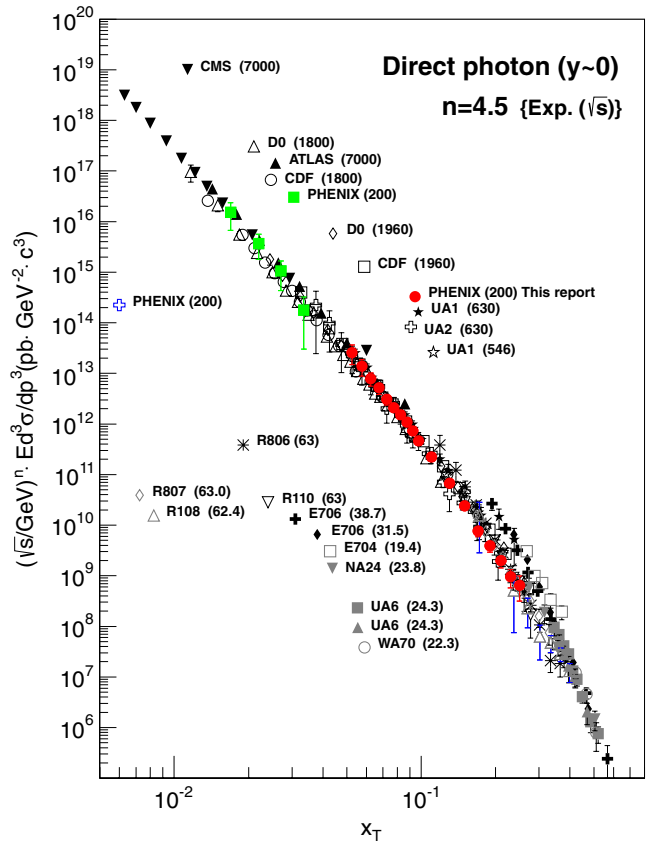

FIG. 14 (color online). Various direct photon cross section measurements in $p+p$ and $p+\bar{p}$ collisions scaled by $(\sqrt{s})^{4.5}$ vs $x_T \equiv 2p_T/\sqrt{s}$. The legend shows the experiment and the center-of-mass energy (GeV) in parenthesis. Table I shows the references.

the systematic uncertainty. Explanations of possible discrepancy were thought to be underlying event activity as well as the contribution of photons from quark fragmentation, which are not considered in the theory calculation. However a study with an event generator (PYTHIA tune A [22]) did not show any drop in the low p_T region for the direct photons, while the level of isolated photons from π^0 decays was well reproduced.[3]

V. DISCUSSION

Figure 10 shows good agreement between the data and NLO pQCD calculations. While the calculations at low p_T seem low, the correlated systematic uncertainties in the data are such that the difference is not significant.

Figure 14 compiles this data and other measurements of direct photons in $p+p$ or $p+\bar{p}$ collisions from both

[3]In the previous paper [5], it was claimed that the effect of underlying events was large. At that time, the Monte-Carlo calculation was done only for direct photon process and the ratio was scaled up to the NLO calculation. For the present work, a full mixture of processes was generated, so the result can be directly compared with data, assuming that PYTHIA reproduces the physics correctly.

collider and fixed target experiments, over a broad range of collision energy. Note that most of the collider data except for that of PHENIX apply an isolation cut in their photon selection as listed in Table I. Also note that the PHENIX measurement [32] having the lowest p_T points uses the virtual-photon method. The cross sections are shown as a function of $x_T = 2p_T/\sqrt{s}$ and scaled by the empirical value of $(\sqrt{s})^{n_{\rm eff}}$ with $n_{\rm eff} = 4.5$ [Eq. (9)]. The effective power, $n_{\rm eff}$, is primarily sensitive to the quantum exchange governing the reaction but also has sensitivity to scale breaking. For measurements of single particle or single jet inclusive p_T distributions, this x_T scaling [45,46] provides a data driven test of whether pQCD or some other underlying subprocess is at work, as well as providing a compact quantitative way to describe the data using the effective index, $n_{\rm eff}(x_T, \sqrt{s})$

$$E\frac{d^3\sigma}{dp^3} = \frac{d^3\sigma}{p_T dp_T dy d\phi} = \frac{1}{p_T^{n_{\rm eff}(x_T,\sqrt{s})}} F\left(\frac{p_T}{\sqrt{s}}\right) = \frac{1}{(\sqrt{s})^{n_{\rm eff}(x_T,\sqrt{s})}} G(x_T), \tag{9}$$

where $Ed^3\sigma/dp^3$ is the invariant cross section for inclusive particle production with transverse momentum p_T at c.m. energy $\sqrt{s}$ and $x_T = 2p_T/\sqrt{s}$. It is important to emphasize that the effective power, $n_{\rm eff}(x_T, \sqrt{s})$, is different from the power n of the invariant cross section at any given value of $\sqrt{s}$.

For pure vector gluon exchange, or for QCD without evolution of α_s and the structure and fragmentation functions, $n_{\rm eff} = 4$ as in Rutherford scattering. However, due to the scale breaking in QCD, the measured value of $n_{\rm eff}$ depends on the x_T value and the range of $\sqrt{s}$ used in the computation [46].

For inclusive direct photon production in $p + p$ collisions at midrapidity, if we assume $x_1 = x_2 = x_T$ and $\langle\cos\theta^*\rangle = 0$, then from Eq. (1), the x_T scaled inclusive cross section in pQCD is approximately:

$$(\sqrt{s})^{n_{\rm eff}} E\frac{d^3\sigma}{dp^3} \propto [\sqrt{s}]^{(n_{\rm eff}-4)} \frac{x_T g_p(x_T, Q^2) F_{2p}(x_T, Q^2)\alpha_s(Q^2)}{x_T^4} \propto \frac{x_T g_p(x_T) F_{2p}(x_T)}{x_T^4}, \tag{10}$$

where $x_T g_p$ is the gluon momentum distribution function in the proton and F_{2p} is the proton structure function measured in DIS, and we assume that the empirical value $n_{\rm eff} - 4 = 0.5$ takes account of the scale breaking effects. The x_T scaling of all the available data, with some exception at low $\sqrt{s}$, is impressive. As one goes to higher x_T, the power of the invariant cross section becomes softer. Figure 14 gives the same information as the agreement with the pQCD calculations [4], but in addition shows the validity of pQCD directly from the data by a simple but powerful scaling rule. The value of $n_{\rm eff} = 4.5$ is consistent

TABLE I. Experimental data for Fig. 14. Points consistent with 0 are excluded from the plot. Reference [23] is a good review.

System	Experiment [Ref.]	$\sqrt{s}$ [GeV]	E_T range [GeV]	η or x_F range	Iso cut	Data points
$p + p$	CMS [24]	7000	22–210	$\lvert\eta\rvert < 1.45$	yes	11
$p + p$	ATLAS [25]	7000	50–300	$\lvert\eta\rvert < 0.6$	yes	8
$p\bar{p}$	D0 [26]	1800	10.5–108.4	$\lvert\eta\rvert < 0.9$	yes	23
$p\bar{p}$	D0 [27,28]	1960	23.9–256	$\lvert\eta\rvert < 0.9$	yes	17
$p\bar{p}$	CDF [29,30]	1800	12.3–114.7	$\lvert\eta\rvert < 0.9$	yes	16
$p\bar{p}$	CDF [31]	1960	32–350	$\lvert\eta\rvert < 1.0$	yes	16
$p + p$	PHENIX [32]	200	1.7–3.3	$\lvert\eta\rvert < 0.35$	no	4
$p + p$	PHENIX (this work)	200	5.3–25	$\lvert\eta\rvert < 0.25$	no	18
$p + p$	PHENIX [5]	200	3.75–15	$\lvert\eta\rvert < 0.25$	no	16
$p\bar{p}$	UA1 [33]	630	17–90	$\lvert\eta\rvert < 0.8$	yes	16
$p\bar{p}$	UA1 [33]	546	17–46	$\lvert\eta\rvert < 0.8$	yes	6
$p\bar{p}$	UA2 [34]	630	15.9–82.3	$\lvert\eta\rvert < 0.76$	yes	13
$p + p$	R110 [35]	63	4.7–8.7	$\lvert\eta\rvert < 0.8$	yes	7
$p + p$	R806 [36]	63	3.75–11.50	$\lvert\eta\rvert < 0.2$	yes	14
$p + p$	R807 [37]	63	4.75–10.36	$\lvert\eta\rvert < 0.7$	yes	11
$p + p$	R108 [38]	62.4	5.37–12.44	$\lvert\eta\rvert < 0.45$	yes	8
$p + p$	E706 [39]	38.8	3.8–11	$-1. < \eta < 0.5$	no	9
$p + p$	E706 [39]	31.6	3.8–9	$-0.75 < \eta < 0.75$	no	8
$p + p$	E704 [40]	19.4	2.6–3.6	$\lvert x_F\rvert < 0.15$	yes	5
$p + p$	NA24 [41]	23.8	3.3–6	$-0.65 < \eta < 0.52$	no	5
$p + p$	WA70 [42]	23.0	4.1–5.7	$\lvert x_F\rvert < 0.05$	no	5
$p + p$	UA6 [43]	24.3	4.2–6.3	$-0.1 < \eta < 0.9$	no	9
$p\bar{p}$	UA6 [44]	24.3	4.2–5.7	$-0.1 < \eta < 0.9$	no	6

with previous analyses of x_T scaling in direct-γ production [35,47,48].

VI. SUMMARY AND CONCLUSIONS

The invariant differential cross section for the production of direct photons in $p + p$ collisions at $\sqrt{s} = 200$ GeV at midrapidity was measured. It extends the p_T reach up to 25 GeV/c. An NLO pQCD calculation agrees well with the measurement, supporting the validity of such calculations.

The effect of an isolation cut on the direct photon cross section was measured to be negligible ($< 10\%$) in agreement with NLO theoretical calculations. The isolation cut enhances the $g + q \to \gamma + q$ contribution and suppresses a possible background of single photons from bremsstrahlung or jet fragmentation. The main utility of the isolation cut is that it reduces the background of photons from hadronic decays by a significant factor of $\sim 60\%$. Furthermore, the data are an important reference for interpreting direct photon spectra in heavy-ion collisions.

ACKNOWLEDGMENTS

We thank the staff of the Collider-Accelerator and Physics Departments at Brookhaven National Laboratory and the staff of the other PHENIX participating institutions for their vital contributions. We also thank Werner Vogelsang for providing calculations and for valuable, in-depth discussions. We acknowledge support from the Office of Nuclear Physics in the Office of Science of the Department of Energy, the National Science Foundation, a sponsored research grant from Renaissance Technologies LLC, Abilene Christian University Research Council, Research Foundation of SUNY, and Dean of the College of Arts and Sciences, Vanderbilt University (U.S.A), Ministry of Education, Culture, Sports, Science, and Technology and the Japan Society for the Promotion of Science (Japan), Conselho Nacional de Desenvolvimento Científico e Tecnológico and Fundação de Amparo à Pesquisa do Estado de São Paulo (Brazil), Natural Science Foundation of China (P. R. China), Ministry of Education, Youth and Sports (Czech Republic), Centre National de la Recherche Scientifique, Commissariat à l'Énergie Atomique, and Institut National de Physique Nucléaire et de Physique des Particules (France), Ministry of Industry, Science and Tekhnologies, Bundesministerium für Bildung und Forschung, Deutscher Akademischer Austausch Dienst, and Alexander von Humboldt Stiftung (Germany), Hungarian National Science Fund, OTKA (Hungary), Department of Atomic Energy and Department of Science and Technology (India), Israel Science Foundation (Israel), National Research Foundation and W. C. U. program of the Ministry Education Science and Technology (Korea), Ministry of Education and Science, Russian Academy of Sciences, Federal Agency of Atomic Energy (Russia), V. R. and the Wallenberg Foundation (Sweden), the U.S. Civilian Research and Development Foundation for the Independent States of the Former Soviet Union, the U.S.-Hungarian Fulbright Foundation for Educational Exchange, and the U.S.-Israel Binational Science Foundation.

APPENDIX

Here we show Tables II, III, IV, V, VI, and VII of the measured invariant differential cross section, the ratio of isolated to inclusive direct photon, and systematic uncertainties.

TABLE II. Cross section of midrapidity inclusive direct photon production in $p + p$ collisions at $\sqrt{s} = 200$ GeV as a function of transverse momentum (p_T). Asymmetric statistical uncertainties occur in p_T bins with no tagged π^0 counts.

p_T [GeV/c]	$Ed^3\sigma/dp^3$ [pb·GeV^{-2}·c^3]	Stat−	Stat+	Syst
5.25	1.14e + 03	3.04e + 01	3.04e + 01	4.78e + 02
5.75	6.13e + 02	1.92e + 01	1.92e + 01	2.21e + 02
6.25	3.48e + 02	1.27e + 01	1.27e + 01	1.01e + 02
6.75	2.31e + 02	8.50e + 00	8.50e + 00	6.24e + 01
7.25	1.36e + 02	6.12e + 00	6.12e + 00	3.13e + 01
7.75	9.29e + 01	4.41e + 00	4.41e + 00	1.95e + 01
8.25	6.70e + 01	3.22e + 00	3.22e + 00	1.34e + 01
8.75	4.83e + 01	2.45e + 00	2.45e + 00	9.18e + 00
9.25	3.21e + 01	1.89e + 00	1.89e + 00	6.10e + 00
9.75	2.04e + 01	1.46e + 00	1.46e + 00	3.68e + 00
11.00	9.81e + 00	4.23e − 01	4.23e − 01	1.67e + 00
13.00	2.97e + 00	1.89e − 01	1.89e − 01	4.75e − 01
15.00	1.06e + 00	9.85e − 02	9.85e − 02	1.69e − 01
17.00	3.38e − 01	5.51e − 02	5.51e − 02	5.42e − 02
19.00	1.73e − 01	3.37e − 02	3.37e − 02	2.77e − 02
21.00	8.82e − 02	2.06e − 02	2.01e − 02	1.50e − 02
23.00	4.22e − 02	1.52e − 02	1.41e − 02	7.18e − 03
25.00	2.87e − 02	1.41e − 02	9.07e − 03	4.30e − 03

TABLE III. Ratio of isolated/inclusive direct photon (Fig. 13). Upper(+) and lower bounds(−) on systematics can be different, and are listed separately.

$\langle p_T \rangle$ [GeV/c]	Ratio	Stat	Syst+	Syst−
5.23	0.658	0.014	0.217	0.151
5.73	0.690	0.017	0.193	0.145
6.23	0.764	0.022	0.176	0.130
6.73	0.730	0.021	0.124	0.102
7.23	0.793	0.027	0.127	0.103
7.73	0.813	0.029	0.106	0.089
8.23	0.750	0.028	0.074	0.067
8.74	0.742	0.029	0.059	0.052
9.24	0.806	0.035	0.064	0.056
9.74	0.911	0.047	0.073	0.064
10.83	0.863	0.027	0.060	0.052
12.85	0.945	0.040	0.057	0.057
14.87	0.916	0.055	0.046	0.046
16.89	1.082	0.118	0.119	0.097
18.90	1.017	0.119	0.081	0.071
20.91	0.975	0.096	0.039	0.039
22.92	1.114	0.193	0.100	0.100
24.92	0.909	0.091	0.000	0.000

TABLE IV. Ratio of isolated/inclusive photon from π^0 (Fig. 13).

$\langle p_T \rangle$ [GeV/c]	Ratio	Stat	Syst + −
5.22	0.450	0.003	0.018
5.72	0.443	0.003	0.018
6.23	0.433	0.004	0.017
6.73	0.419	0.006	0.017
7.23	0.418	0.007	0.017
7.73	0.409	0.009	0.016
8.23	0.422	0.012	0.017
8.73	0.403	0.014	0.016
9.23	0.392	0.017	0.016
9.73	0.370	0.020	0.015
10.79	0.373	0.015	0.015
12.82	0.372	0.029	0.015
14.84	0.449	0.054	0.018
16.86	0.416	0.083	0.017
18.88	0.619	0.171	0.025
20.89	0.500	0.354	0.020

TABLE V. Components of systematic uncertainties on isolated/inclusive direct photon ratio (expressed as a percentage of the center value). Note that the upper and lower variations are treated separately.

$\langle p_T \rangle$	π^0 count	π^0 correction	Nonphoton	Hadronic decay
5.2	25.1/ − 16.6	20.0/ − 14.3	4.0/ − 3.5	7.7/ − 5.9
5.7	21.6/ − 15.0	16.4/ − 12.4	3.8/ − 3.3	7.1/ − 5.7
6.2	18.7/ − 13.5	10.8/ − 8.8	3.6/ − 3.2	6.9/ − 5.7
6.7	13.8/ − 10.8	7.6/ − 6.6	2.8/ − 2.5	5.2/ − 4.5
7.2	13.1/ − 10.3	5.7/ − 5.1	2.8/ − 2.5	5.3/ − 4.5
7.7	10.7/ − 8.8	4.5/ − 4.1	2.4/ − 2.2	4.5/ − 4.0
8.2	8.4/ − 7.2	3.4/ − 3.2	1.8/ − 1.7	3.4/ − 3.1
8.7	6.8/ − 6.0	2.7/ − 2.6	1.5/ − 1.4	2.9/ − 2.6
9.2	6.6/ − 5.8	2.6/ − 2.5	1.5/ − 1.4	3.0/ − 2.7
9.7	7.0/ − 6.1	2.6/ − 2.5	1.7/ − 1.6	3.4/ − 3.1
10.8	5.3/ − 4.8	2.1/ − 2.0	1.3/ − 1.2	4.0/ − 3.6
12.9	3.8/ − 3.6	1.9/ − 1.8	1.0/ − 0.9	4.6/ − 4.1
14.9	2.9/ − 2.7	1.8/ − 1.7	0.7/ − 0.7	4.0/ − 3.6
16.9	3.5/ − 3.3	3.0/ − 2.9	0.9/ − 0.9	10.4/ − 8.2
18.9	2.0/ − 1.9	2.6/ − 2.5	0.4/ − 0.4	7.3/ − 5.9
20.9	0.9/ − 0.8	2.8/ − 2.7	0.2/ − 0.2	3.1/ − 2.8
22.9	1.0/ − 1.0	7.2/ − 6.3	0.3/ − 0.3	6.5/ − 5.7
24.9	0.0/0.0	0.0/0.0	−0.0/ − 0.0	0.0/0.0

TABLE VI. Systematic uncertainties of inclusive direct photon measurement. The percentage uncertainties of each component shows (A) the global factor (quadrature sum of components A1, A2, and A3), (B) inclusive photon counts, (C) π^0 tagging, (D) the factor for the total π^0 counts, and (E) the factor for the hadron contribution other than π^0) and the contribution to the direct photon signal [A*1, B*W, C*(W-1), D*(W-1), E*(W-1)]. W is the ratio of $N_{\rm incl}/N_{\rm dir}$. Individual components are (A1) energy scale error transformed to the cross section, (A2) acceptance and smearing, (A3) $\sigma_{\rm BBC}$ and BBC trigger bias, (B1) nonvertex, neutral hadron subtraction, (C1) π^0 combinatorial background subtraction, (C2) loss for conversion and Dalitz decay, (D1) $E_{\rm min}$ calibration, (D2) input π^0 spectrum in the MC, (D3) π^0 merge model (correction for the complete merging), (D4) π^0 merge model (cluster shape parametrization in the MC), (D5) Geometry and trigger mask, (E1) ratio of all hadronic decay to π^0 contribution, (E2) isolation with own decay partner, and (E3) π^0 merge correction for other hadron contribution.

p_T	1/W	A1	A2	A3	A*1	B1	B*W	C1	C2	C*(W-1)	D1	D2	D3	D4	D5	D*(W-1)	E1	E2	E*(W-1)	total %
5.25	0.13	10	3	10	14.46	1	7.49	3	1	20.53	4	2	0	0	1	29.74	2	0	12.98	41.71
5.75	0.15	10	3	10	14.46	1	6.47	3	1	17.31	4	2	0	0	1	25.08	2	0	10.94	36.04
6.25	0.18	10	3	10	14.46	1	5.7	3	1	14.86	3	2	0	0	1	17.58	2	0	9.4	29.32
6.75	0.2	10	3	10	14.46	1	5.09	3	1	12.93	3	2	0	0	1	15.3	2	0	8.18	26.52
7.25	0.22	10	3	10	14.46	1	4.6	3	1	11.38	2	2	0	0	1	10.79	2	0	7.2	22.97
7.75	0.24	10	3	10	14.46	1	4.19	3	1	10.1	2	2	0	0	1	9.58	2	0	6.39	21.47
8.25	0.26	10	3	10	14.46	1	3.85	3	1	9.02	2	2	0	0	1	8.56	2	0	5.71	20.28
8.75	0.28	10	3	10	14.46	1	3.57	3	1	8.11	2	2	0	0	1	7.7	2	0	5.13	19.31
9.25	0.3	10	3	10	14.46	1	3.32	3	1	7.33	2	2	0	0	1	6.95	2	0	4.63	18.53
9.75	0.32	10	3	10	14.46	1	3.1	3	1	6.64	2	2	0	0	1	6.3	2	1	4.7	18.01
11	0.38	10	3	10	14.46	1	2.67	3	1	5.27	2	2	0	1	1	5.27	2	2	4.71	17.14
13	0.46	10	3	10	14.46	1	2.18	3	1	3.73	2	2	0	3	1	5	2	3	4.25	16.45
15	0.54	10	3	10	14.46	1	1.84	3	1	2.66	2	2	1.7	4	1	4.44	2	4	3.76	15.92
17	0.63	10	3	10	14.46	1	1.59	3	1	1.88	2	2	3.1	6	1	4.4	2	6	3.76	15.77
19	0.71	10	3	10	14.46	1	1.41	3	1	1.29	2	2	6.7	8	1	4.41	2	8	3.35	15.6
21	0.8	10	3	10	14.46	1	1.26	3	1	0.82	2	2	27.4	10	1	7.56	2	10	2.63	16.59
23	0.88	10	3	10	14.46	1	1.14	3	1	0.44	2	2	56.3	12	1	7.93	2	12	1.67	16.62
25	0.96	10	3	10	14.46	1	1.04	3	1	0.12	2	2	102.8	14	1	3.99	2	13	0.51	15.04

TABLE VII. Systematic uncertainties of isolated direct photon measurement. The percentage uncertainties of each component are as given in the Table VI caption, except that the contributions to the direct photon signal are A*1, B*W0, C*W3, C*W2, D*W1, and E*W1. W0, W1, W2, and W3 are defined in Eq. (8). Individual components A1 through E3 are also as given in the Table VI caption.

p_T	W0	W1	W2	W3	A1	A2	A3	A*1	B1	B*W0	C1	C2	C*W3	C*W2	D1	D2	D3	D4	D5	D*W1	E1	E2	E3	E*W1	Total %
5.25	3.69	4.16	0.1	2.62	10	3	10	14.46	1	3.69	3	1	8.3	0.3	4	2	0	0	1	19.07	2	0.1	0	8.33	26.92
5.75	3.09	3.27	0.09	1.98	10	3	10	14.46	1	3.09	3	1	6.27	0.3	4	2	0	0	1	14.99	2	0.1	0	6.55	22.92
6.25	2.65	2.62	0.09	1.53	10	3	10	14.46	1	2.65	3	1	4.83	0.29	3	2	0	0	1	9.79	2	0.3	0	5.29	19.06
6.75	2.32	2.13	0.09	1.2	10	3	10	14.46	1	2.32	3	1	3.8	0.29	3	2	0	0	1	7.96	2	0.3	0	4.3	17.63
7.25	2.08	1.76	0.09	0.96	10	3	10	14.46	1	2.08	3	1	3.04	0.28	2	2	0	0	1	5.27	2	0.4	0	3.58	16.23
7.75	1.89	1.47	0.09	0.78	10	3	10	14.46	1	1.89	3	1	2.48	0.28	2	2	0	0	1	4.42	2	0.5	0	3.04	15.73
8.25	1.75	1.25	0.09	0.65	10	3	10	14.46	1	1.75	3	1	2.06	0.27	2	2	0	0	1	3.76	2	0.6	0	2.61	15.41
8.75	1.64	1.08	0.08	0.55	10	3	10	14.46	1	1.64	3	1	1.73	0.27	2	2	0	0	1	3.24	2	0.7	0	2.29	15.18
9.25	1.56	0.94	0.08	0.47	10	3	10	14.46	1	1.56	3	1	1.48	0.26	2	2	0	0	1	2.82	2	0.7	0	1.99	15.02
9.75	1.49	0.83	0.08	0.41	10	3	10	14.46	1	1.49	3	1	1.28	0.26	2	2	0	0	1	2.49	2	0.9	0	1.82	14.91
11	1.37	0.63	0.08	0.3	10	3	10	14.46	1	1.37	3	1	0.95	0.24	2	2	0	1	1	2	2	1	1	1.55	14.77
13	1.27	0.46	0.07	0.21	10	3	10	14.46	1	1.27	3	1	0.66	0.23	2	2	0	3	1	1.94	2	1.5	2	1.46	14.73
15	1.22	0.36	0.07	0.16	10	3	10	14.46	1	1.22	3	1	0.51	0.21	2	2	1.7	4	1	1.89	2	2.3	3	1.53	14.72
17	1.2	0.29	0.06	0.13	10	3	10	14.46	1	1.2	3	1	0.41	0.19	2	2	3.1	6	1	2.12	2	3.2	4	1.58	14.75
19	1.18	0.22	0.06	0.1	10	3	10	14.46	1	1.18	3	1	0.32	0.18	2	2	6.7	8	1	2.43	2	4.3	6	1.71	14.81
21	1.15	0.16	0.05	0.07	10	3	10	14.46	1	1.15	3	1	0.23	0.17	2	2	27.4	10	1	4.73	2	5.4	8	1.59	15.34
23	1.12	0.1	0.05	0.04	10	3	10	14.46	1	1.12	3	1	0.14	0.15	2	2	56.3	12	1	5.85	2	6.5	9	1.14	15.68
25	1.09	0.05	0.05	0.02	10	3	10	14.46	1	1.09	3	1	0.07	0.14	2	2	102.8	14	1	5.48	2	7.5	10	0.67	15.51

[1] H. Fritzsch and P. Minkowski, Phys. Lett. **69B**, 316 (1977).
[2] A. Adare *et al.* (PHENIX Collaboration), Phys. Rev. D **82**, 072001 (2010).
[3] A. Adare *et al.* (PHENIX Collaboration), Phys. Rev. C **80**, 024908 (2009).
[4] P. Aurenche, J. P. Guillet, E. Pilon, M. Werlen, and M. Fontannaz, Phys. Rev. D **73**, 094007 (2006).
[5] S. S. Adler *et al.* (PHENIX Collaboration), Phys. Rev. Lett. **98**, 012002 (2007).
[6] K. Adcox *et al.* (PHENIX Collaboration), Nucl. Instrum. Methods Phys. Res., Sect. A **499**, 469 (2003).
[7] S. S. Adler *et al.* (PHENIX Collaboration), Phys. Rev. Lett. **91**, 241803 (2003).
[8] A. Adare *et al.* (PHENIX Collaboration), Phys. Rev. D **79**, 012003 (2009).
[9] GEANT 3.2.1 Manual (1994), CERN W5013, URL http://wwwasdoc.web.cern.ch/wwwasdoc/pdfdir/geant.pdf.
[10] A. Adare *et al.* (PHENIX Collaboration), Phys. Rev. D **83**, 032001 (2011).
[11] A. Adare *et al.* (PHENIX Collaboration), Phys. Rev. D **83**, 052004 (2011).
[12] L. E. Gordon and W. Vogelsang, Phys. Rev. D **48**, 3136 (1993).
[13] L. E. Gordon and W. Vogelsang, Phys. Rev. D **50**, 1901 (1994).
[14] P. Aurenche, A. Douiri, R. Baier, M. Fontannaz, and D. Schiff, Phys. Lett. **140B**, 87 (1984).
[15] P. Aurenche, R. Baier, M. Fontannaz, and D. Schiff, Nucl. Phys. **B297**, 661 (1988).
[16] H. Baer, J. Ohnemus, and J. F. Owens, Phys. Rev. D **42**, 61 (1990).
[17] H. Baer, J. Ohnemus, and J. F. Owens, Phys. Lett. B **234**, 127 (1990).
[18] J. Pumplin, D. R. Stump, J. Huston, H.-L. Lai, P. Nadolsky, and W.-K. Tung, J. High Energy Phys. 07 (2002) 012.
[19] L. Bourhis, M. Fontannaz, and J. Ph. Guillet, Eur. Phys. J. C **2**, 529 (1998).
[20] A. Adare *et al.* (PHENIX Collaboration), Phys. Rev. D **76**, 051106 (2007).
[21] M. Gluck, E. Reya, and A. Vogt, Phys. Rev. D **48**, 116 (1993).
[22] T. Sjostrand, Report No. CERN-TH-7112, 1994, http://cdsweb.cern.ch/record/287231?ln=en.
[23] W. Vogelsang and M. R. Whalley, J. Phys. G **G23**, A1 (1997).
[24] V. Khachatryan *et al.*, Phys. Rev. Lett. **106**, 082001 (2011).
[25] G. Aad *et al.* (ATLAS Collaboration), Phys. Lett. B **706**, 150 (2011).
[26] S. Abachi *et al.* (D0 Collaboration), Phys. Rev. Lett. **77**, 5011 (1996).
[27] V. Abazov *et al.* (D0 Collaboration), Phys. Lett. B **639**, 151 (2006).
[28] V. Abazov *et al.* (D0 Collaboration), Phys. Lett. B **658**, 285(E) (2008).
[29] F. Abe *et al.* (CDF Collaboration), Phys. Rev. Lett. **73**, 2662 (1994).
[30] F. Abe *et al.* (CDF Collaboration), Phys. Rev. Lett. **74**, 1891(E) (1995).
[31] T. Aaltonen *et al.* (CDF Collaboration), Phys. Rev. D **80**, 111106 (2009).
[32] A. Adare *et al.* (PHENIX Collaboration), Phys. Rev. C **81**, 034911 (2010).
[33] C. Albajar *et al.* (UA1 Collaboration), Phys. Lett. B **209**, 385 (1988).
[34] J. Alitti *et al.* (UA2 Collaboration), Phys. Lett. B **288**, 386 (1992).
[35] A. L. S. Angelis *et al.* (CMOR Collaboration), Nucl. Phys. **B327**, 541 (1989).
[36] E. Anassontzis *et al.*, Z. Phys. C **13**, 277 (1982).
[37] T. Akesson *et al.* (Axial Field Spectrometer Collaboration), Sov. J. Nucl. Phys. **51**, 836 (1990), http://cdsweb.cern.ch/record/200242?ln=en.
[38] A. L. S. Angelis *et al.* (CCOR Collaboration), Phys. Lett. **94B**, 106 (1980).
[39] L. Apanasevich *et al.* (FNAL E706 Collaboration), Phys. Rev. D **70**, 092009 (2004).
[40] D. L. Adams *et al.* (E704 Collaboration), Phys. Lett. B **345**, 569 (1995).
[41] C. De Marzo *et al.* (NA24 Collaboration), Phys. Rev. D **36**, 8 (1987).
[42] M. Bonesini *et al.* (WA70 Collaboration), Z. Phys. C **38**, 371 (1988).
[43] G. Ballocchi *et al.* (UA6 Collaboration), Phys. Lett. B **436**, 222 (1998).
[44] G. Sozzi *et al.* (UA6 Collaboration), Phys. Lett. B **317**, 243 (1993).
[45] R. Blankenbecler, S. J. Brodsky, and J. F. Gunion, Phys. Lett. **42B**, 461 (1972).
[46] R. F. Cahalan, K. A. Geer, J. B. Kogut, and L. Susskind, Phys. Rev. D **11**, 1199 (1975).
[47] M. J. Tannenbaum, Proc. Sci. [CFRNC2006] 001 (2006), http://pos.sissa.it/archive/conferences/030/001/CFRNC2006_001.pdf.
[48] D. dÉnterria and J. Rojo, Nucl. Phys. **B860**, 311 (2012).